ESKİŞEHİR TEKNİK ÜNİVERSİTESİ BİLİM VE TEKNOLOJİ DERGİSİ B- TEORİK BİLİMLER

Eskişehir Technical University Journal of Science and Technology B- Theoritical Sciences

2018, 6(2), pp. 235 - 242, DOI: 10.20290/aubtdb.462839

TiO_2 FILMS WITH VARIOUS CRYSTAL STRUCTURES FOR SINGLE AND BILAYER PHOTOANODES OF DYE-SENSITIZED SOLAR CELLS

Nursev ERDOĞAN [1, 2, *], Jongee PARK [3], Abdullah ÖZTÜRK [1]

[1] Metallurgical and Materials Engineering Department, Middle East Technical University, Turkey
[2] Advanced Materials, Process and Energy Technology Center, Turkish Aerospace Industry Inc., Ankara, Turkey
[3] Metallurgical and Materials Engineering Department, Atılım University, Ankara, Turkey

ABSTRACT

Phase pure and composite TiO_2 nanopowders exhibiting various crystal structures (anatase, rutile and brookite) are used as photoanode in dye-sensitized solar cells. The nanopowders are deposited in paste form onto a conducting oxide glass using doctor blade method in single layer and bilayers. The highest solar efficiency achieved by the single layer photoanode composed of > 99 wt % anatase crystals was 2.86 %. The solar efficiency of 4.93 % has been harvested via bilayer photoanode built by applying a layer consisting 55 wt % anatase and 45 wt % rutile phase nanoparticles on top of the layer composed of a mixture of > 99 wt % anatase crystals. The improved photovoltaic performance is attributed to anatase dominated bottom layer which facilitates electron charge generation with high surface area and charge transport by proper crystal structure as well as synergistic effect of binary phase content of the photoanodes. The porous structure of top layer enhances diffusion of the I^-/I_3^- electrolyte in the bilayer TiO_2 photoanode.

Keywords: Titanium dioxide, Dye-sensitized solar cells, Bilayer photoanode, Nanoparticles

1. INTRODUCTION

Photovoltaic technology is of interest for a wide range of applications in the fabrication of small solar devices as well as large-scale systems. Harvesting solar energy is very crucial for operating extra-terrestrial spacecraft, stations, and satellites that are produced using the highest quality materials to ensure reliability and long-term stability. Traditional solar technology is reaching its theoretical limits of meeting the power generation needs of future space technologies [1, 2]. Dye-Sensitized solar cells (DSSCs) are new generation solar cells with comparable efficiency considering its low cost. In a typical DSSC, the photo-excited electrons of the dye molecules are transferred to the semiconductor conduction band, which are afterwards transferred to the external circuit. Since the breakthrough in the solar efficiency of 11% reported by O'Regan and Gratzel in 2005 [3], many modifications including materials used in sensitizing dye, electrolyte, counter electrode, and photoanode have been made to increase the efficiency [4].

Anatase is a well-known polymorph of TiO_2 which is used to get high performance in DSSCs. However, synergistic effect of two or more polymorphs of TiO_2 is also known to enhance opto-electronic efficiency of DSSCs [5]. The TiO_2 films consisting of a mixture of anatase and rutile phases significantly increase photocurrent and overall solar conversion efficiency. Ternary phase systems are even more effective [6]. Shen et al. reported 7.24 % efficiency using ternary anatase, C-doped rutile, and C doped brookite structures [7]. An advance technology using a core shell binary phase was also introduced to overcome charge transport [8].

The purpose of this study was to examine photovoltaic performance of TiO_2 nanoparticles in various crystal structures for the photoanodes to be used in DSSC in single layer and bilayer form. Nanoparticles

*Corresponding Author: abdullah@metu.edu.tr
Received: 14.04.2018 Accepted: 25.09.2018

comprising different proportions of anatase, rutile, and brookite phases were applied to understand the effect of interaction of these powders on solar efficiency.

2. EXPERIMENTAL

2.1. Materials

TiO_2 powders used in the preparation of photoanodes were synthesized by hydrothermal method. Details of the production procedure and the characteristics of the powders are given elsewhere [9]. Ethyl cellulose (46 % ethoxyl), α-Terpineol (90 %), Ethanol (96.0-97.2 %), Citric acid (99 %), Chloroplatinic acid hydrate (≥99.9 %) were purchased from Sigma Aldrich with product numbers 200670, 432628, 24105, C0759, respectively. Acetic acid (100 %) was puchased from Merck with product number 100056. Fluorine-doped tin oxide (FTO) transparent conducting glass substrates (15-20 Ω/sq) were supplied from Kintec, Korea.

2.2. Photoanode Preparation

The TiO_2 pastes were prepared according to approach proposed by Ito et al. using the powders synthesized by hydrothermal route [10]. Code of the powders regarding the synthesis conditions and the proportions of the crystalline phases present in the powders is given in Table 1.

The pastes prepared were coded with respect to the powder used. The letter P was inserted in front of the powder code implying that the paste is formed from that powder. Pastes were applied onto a FTO glass by doctor blade method in an active area of 1 cm^2. Paste coated FTO glass was sintered at 500 ºC for 30 min. The photoanodes were named according to the codes of the pastes used to built photoanodes. Binary photoanodes were prepared using paste P3 as bottom layer and pastes P1, P3, P4, and P5 as top layer. In order to code binary photoanodes numbers were used in the order of paste placement. The letter C was added to coding when the photoanode was used for cell preparation.

Table 1. Code of the powders, their synthesis conditions and the proportions of the phases present.

Powder Code	Synthesis Conditions			Phase Content (wt %)			Surface Area (m^2/g)
	Temperature (ºC)	Time (h)	Catalyzer Molarity (M)	Anatase	Rutile	Brookite	
1	110	6	1	86	8	6	226
2*	130	36	10	>99	-	-	113
3	140	6	8	>99	-	-	248
4**	140	3	8	-	>99	-	148
5	140	3	8	55	45	-	192

* Protonation and calcination at 500 ºC were applied following synthesis.

**H titanate powder was used as nucleation seed during synthesis.

Dye loading was done using 0.5 mM dye solution when the photoanodes were at 80 ºC. N719 dye was used as sensitizer. Counter electrode was prepared using Pt solution through dip coating onto an FTO glass that had two holes. Then, counter electrode was activated by heating at 450 ºC for 30 min. After activation, the activated counter electrode was immediately assembled to the cell in order not to lose its catalytic effect. The electrodes were sealed using Surlyn film® melted with a heating gun at 100 ºC. After that, electrolyte was filled through one of the hole in counter electrode while air was taken off from the other hole. Finally, the holes were closed using Surlyn film®.

2.3. Characterization

The structures synthesized were detected using an X-ray diffractometer (Rigaku, D/MAK/B). The phase composition, purity, and crystallinity of all the samples were identified through X-Ray diffraction

(XRD) analysis in continuous scan mode at a rate of 0.03 °/s. XRD patterns were analyzed using Rigaku 4.2 software to identify the crystalline phase(s) present in the products. The XRD patterns were presented in another publication [9]. Surface area of the powders was measured using Quantachrome Corporation, Autosorb-6 by multi point Brunauer, Emmett and Teller (BET) method. Optical Transmittance was conducted using UV-Vis Spectrophotometer (Scinco). Electrochemical impedance spectroscopy (EIS) analysis was performed using Gamry EIA 3000 potentiostat biased to Philips White LED Lamp (25 W). The signals were collected between 100 kHz and 10 mHz. The scan amplitude was 10 mV. DC current of 0.6 V was applied to the cells. The J-V measurements were conducted under AM 1.5 G illumination with a solar simulator (Newport) equipped with a 100 W Xenon lamp.

3. RESULTS AND DISCUSSION

3.1 Optical Properties

Absorbance data of N719 dye with respect to wavelength in various molarities were determined using UV-Vis photospectrometer. The experiment was conducted 3 times with gradually increasing dye molarity from 0.05 to 0.2 M to get an equation that correlates absorbance and molarity at the absorbance value of 532 nm. The equation given below was anticipated.

$$y=12.314x+0.13 \quad (1)$$

where, x is the molarity of desorbed dye from photoanodes and y is the absorbance of solution at 532 nm.

Thickness of sintered anodes is shown in Table 2. Dye adsorption of powders is calculated using eqn. (1). The amount of desorbed dye from photoanodes using NaOH aqua solution is given in Table 2. The highest adsorption is realized by P2 that consists of anatase crystal structure dominantly. The powder has titanate crystal structure before calcination to obtain anatase that is popular with its negative surface charge. Any residual titanate structure may enhance the affinity to cationic N719 dye. For the powders containing rutile phase, dye adsorption falls gradually. Reduced adsorption is probably due to lower surface activity of rutile phase as compared to that of anatase and brookite phases. However, the lowest adsorption implemented by P5. Although the anatase existence in the structure, dye adsorption is lower than phase pure rutile in P5. This result can be relevant to agglomerated structure of P5, which decreases surface area.

Table 2. Thickness and desorbed dye per volume of sintered anodes.

Photoanode ($1\ cm^2$)	Thickness (μm)	Desorbed dye (mol/cm^3)
P1	13.57	$1.23x10^{-4}$
P2	8.98	$1.53x10^{-4}$
P3	10.59	$1.45x10^{-4}$
P4	12.46	$1.08x10^{-4}$
P5	12.48	$1.02x10^{-4}$

Figure 1 shows the transmission spectra of the semiconductor single layer formed from the pastes. The lowest transmission obtained by P4 as seen in Figure 1 (a) is probably due to high refractive index and scattering effect inside the structure by rutile phase. P5 shows higher transmission caused by less rutile content as compared to P4 as indicated in Figure 1 (b). P1 and P3 have similar transmission spectra due to the presence of large amount of anatase phase as shown in Figures 1 (c) and (d), respectively. P3 consists of more amount of anatase phase as compared to P1 so that it results in higher transmittance at lower wavelength due to higher valance band maximum of anatase phase. P2 exhibited the maximum transmission as shown in Figure 1 (e).

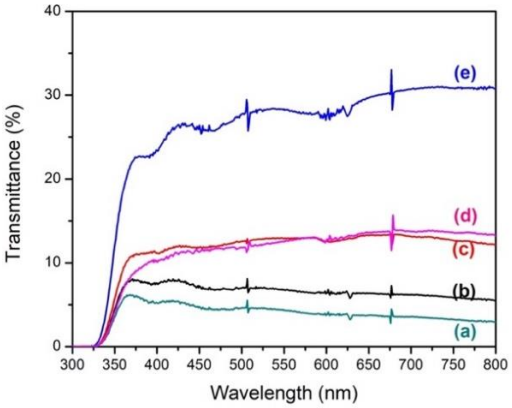

Figure 1. Transmittance spectra of photoanodes (a) P4, (b) P5, (c) P1, (d) P3, and (e) P2.

3.2. Photovoltaic Performance

Figure 2 shows the J-V curves of the cells prepared by using the pastes characterized. Data gained from the curves was tabulated in Table 3. As indicted in Figure 2 (a), the lowest V_{oc} was obtained by PC4. Although rutile structure is reported to have comparable V_{oc} with anatase structure by architecting the morphology [11], V_{oc} of PC4 is the lowest among the 5 cells fabricated in the present study. The low V_{oc} and I_{sc} might be due to rutile content. Kambe and co-workers [12] declared that the diffusion coefficient of conduction band electrons in rutile is significantly lower than that in anatase.

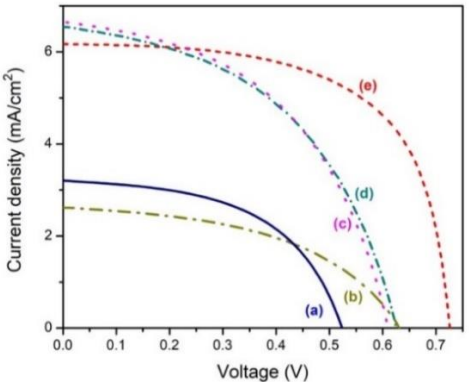

Figure 2. J-V curves of single layer photoanodes (a) PC4, (b) PC2, (c) PC5, (d) PC1, and (e) PC3.

J-V curve of PC2 showed slightly lower current and higher voltage as shown in Figure 2 (b). PC2 led higher voltage as compared to PC4 probably due to its anatase content. Because the conduction band of anatase is 0.2 V more negative than that of rutile, a larger photovoltage could be obtained on anatase than on rutile when the same redox mediator is employed.

J-V plot of PC5 is shown in Figure 2 (c). This photoanode includes both anatase and rutile phases in the structure. Large amount of anatase increased V_{oc} and I_{sc} so that the values were bigger as compared to previous photoanodes. Binary phase crystallized in a core shell structure of this photoanode may be useful for increasing current and voltage by synergistic effect [5,8]. When J-V curve of PC1 shown in Figure 2 (d) was examined, current density increases as compared to other cells and V_{oc} is close to that of PC2. The addition of rutile increases the photocurrent and overall solar efficiency of photoanodes composed of only anatase phase due to synergistic effect. Besides anatase and rutile, brookite may also present in the system. Shen et al. [7] reported 7.24 % efficiency with anatase, C doped rutile, and brookite phase mixture. PC3 showed the maximum V_{oc} as shown in Figure 2 (e). In DSSCs, an increase in the open circuit voltage at a given charge density implies an upward shift of Fermi level. Anatase

content of > 99 wt % and good interaction between particles by well sintering in this sample may result in far larger V_{oc} compared to other cells.

Table 3. Data calculated using J-V curves shown in Figure 2.

Paste	V_{oc} (V)	J_{sc} (mA/cm^2)	V_{max} (V)	I_{max} (mA)	FF (%)	η (%)
PC1	0.62	6.61	0.42	4.56	47	1.92
PC2	0.62	2.62	0.48	1.63	47	0.78
PC3	0.73	6.17	0.64	4.48	66	2.86
PC4	0.52	3.21	0.37	2.39	52	0.88
PC5	0.61	6.68	0.41	4.42	45	1.82

Figure 3 shows J-V curves of the DSSCs fabricated by using composite pastes in binary films. Data obtained from the curves are tabulated in Table 4. The J-V curve of the DSSC composed of P3 as bottom layer and P4 as top layer is shown in Figure 3 (a). Photocurrent density and voltage are both larger than the values obtained for PC4 but lower than that for PC3. The efficiency of 1.10 % was calculated. J-V plot of PC31 is depicted in Figure 3 (b). Binary photoanode built from P1 as top layer and P3 as bottom layer seemed to increase light harvesting. It benefits from more photons by top layer and increase electron diffusion by bottom layer. Photocurrent measured is smaller than the J_{sc} of both photoanodes in single layer. (See Table 4). Measured V_{oc} of 0.63 V is larger than that of PC1 in single layer. FF of the cell is very small so that it yields overall efficiency as low as 1.80 %. Ternary phase mixture on top layer may be detrimental which causes traps for electron recombination in contrast to useful synergistic effect of binary phase mixture.

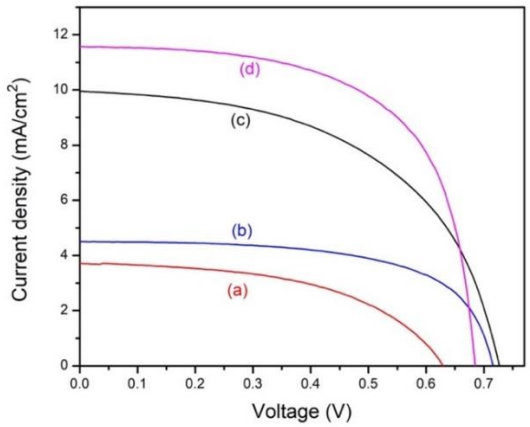

Figure 3. J-V plots of binary layer photoanodes (a) PC34, (b) PC31, (c) PC33, and (d) PC35.

Table 4. Data calculated by J-V plots shown in Figure 6.

Photoanodes	V_{oc} (V)	J_{sc} mA(cm^2)	V_{max} (V)	I_{max} (mA)	FF (%)	η (%)
PC31	0.71	4.49	0.63	2.87	57	1.80
PC33	0.73	9.72	0.55	6.76	52	3.72
PC34	0.63	3.58	0.50	2.19	48	1.10
PC35	0.68	11.51	0.53	9.31	63	4.93

The J-V curve of the DSSC built by P3 as bottom and top layer is indicated in Figure 3 (c). This cell shows a larger I_{sc} as compared to its single layer counterpart. Efficiency also increased more than 10 % caused by increasing photon harvesting by thicker film. DSSC built by P3 as bottom layer and P5 as top layer is depicted in Figure 3 (d). The highest FF is a result of lowest sheet resistance and highest shunt resistance. The cell showed lower V_{oc} as compared to PC3 and PC33 probably due to rutile content of composite binary film. The highest I_{sc} was generated by this composite cell, which is considered to be as a result of increase in light scattering by rutile crystal structure. Although the lowest dye adsorption

was obtained by PC5, probably compatibility between two films prevented recombination and provided a safe travel for the charges.

3.3. EIS Analysis

Figure 4 shows the EIS measurements of cells with single layer paste. R_1, R_2, R_3, and R_4 values tabulated in Table 6 were realized by fitting the curves with the model proposed by Gratzel et. al. [13]. According to the proposed model, R_1 represents the sheet resistance that induced by FTO, electrolyte layer and counter electrode. R_2 represents the charge transfer resistances related to recombination of electrons at the Pt and electrolyte interface and the electron transport resistance. R_3 and R_4 are the charge transfer resistances associated with recombination of electron transport resistance in the system. As indicated in Table 5, R_1 of photoanodes is nearly 20 Ω. R_2 values are ranging between 1-2.3 Ω. The unstable R_2 is considered to be because of activation loss discrepancies due to duration variations until the measurements are complete. In terms of photoanode characterization, R_3 and R_4 are important. The lowest R_4 yielded by PC3 is 11.8 Ω as shown in Figure 4 (a). R_3 is 4.2 Ω. The data obtained by EIS measurements is well fitted with the model. Photovoltaic measurements implied the highest efficiency as indicated in Table 4. R_4 is 39.9 Ω whereas R_3 is 3.1 Ω as indicated in Figure 4 (b).

In terms of R_4, the obtained results confirm photovoltaic performance. The reduced R_3 as compared to PC3 does not decrease the efficiency. As the gap between R_3 and R_4 increases, the fitting shows one large peak. It is valid for also PC5 as shown in Figure 4 (c). Increasing R_3 and R_4 resulted in lower efficiency. PC4 indicates far larger R_4 as compared to previous cells as shown in Figure 4 (d). This is probably due to low interaction between the particles. Rutile crystal structure is also considered effective on increasing charge transfer resistance. R_3 also increases slightly. Regression of fitting is smaller in this cell probably due to R_2 fitting. As the resistance values attributed to charge transfer, R_2 could not be detected clearly reversely in the case of previous cells. The highest R_3 and R_4 were obtained by sample PC2 probably due to lack of interaction between particles. The result is compatible with I-V data that revealed the lowest current and efficiency. Large R_4 shows low recombination between particles and electrolyte, which might seem as an advantage but low transportation also affects current undesirably.

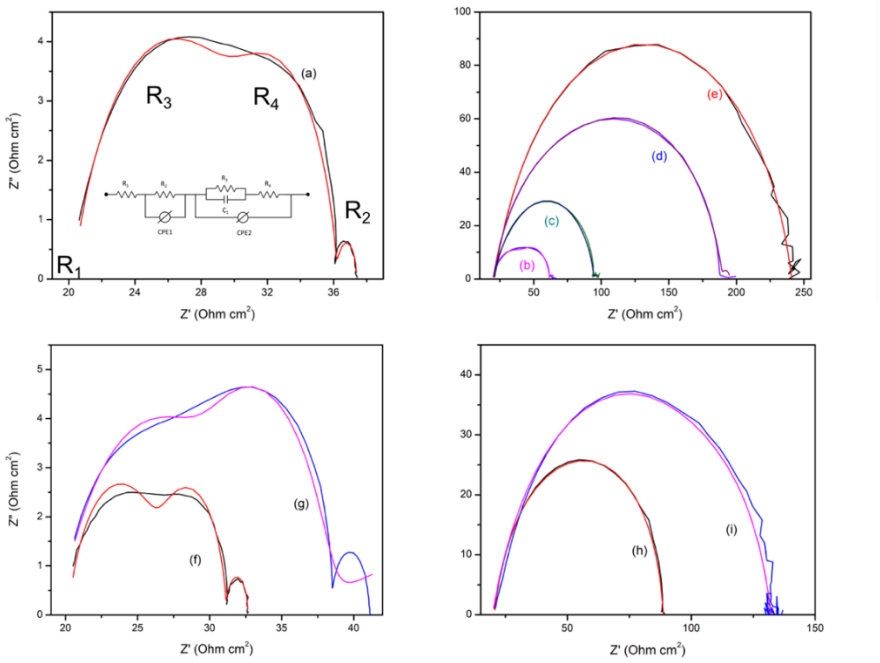

Figure 4. Electrochemical impedance spectroscopy (Nyquist plots) for DSSCs based on single and bilayer photoanodes (a) PC3, (b) PC1, (c) PC5, (d) PC4, (e) PC2, (f) PC35, (g) PC33, (h) PC31, and (i) PC35.

Table 5. EIS parameters for the DSSCs fabricated by single layer photoanodes.

Photoanode	R_1 (Ω)	R_2 (Ω)	R_3 (Ω)	R_4 (Ω)
PC1	20.08	1.2	3.1	39.9
PC2	20.22	2.1	38.0	186.3
PC3	20.63	1.1	4.2	11.7
PC4	20.43	1.9	31.5	142.0
PC5	20.96	1.8	17.2	57.7

The cell with bilayer photoanode PC35 shows the least R_4 as illustrated in Table 6. Fitting perfectly matches with raw data as shown in Figure 4 (f). R_3 is higher than PC3. However, smallest R_4 is consistent with highest efficiency found in photovoltaic measurement. PC33 shows close performance with its single layer form in the EIS analysis as shown in Figure 4 (g). The increase in R_3 is ascribed to increasing pathway of the charges with increasing thickness. The decrease in R_4 is in accordance with increasing efficiency shown in Table 6. Figure 4 (h) depicts the EIS plot of PC31. R_3 and R_4 increase to 6.4 and 62.5 Ω, respectively. These values are even more than the values obtained in single layer P1. This negative result is attributed to low consistency between the films probably in terms of crystallographic behaviour for charge transport. EIS plot of PC34 shown in Figure 4 (i) performed the largest R_4 among the cells fabricated using bilayer photoanodes. The negative result is in agreement with photovoltaic performance of the same cell and also attributed to low consistency between the films probably in terms of crystallographic behaviour for charge transport.

Table 6. EIS parameters for the DSSCs fabricated by bi-layer photoanodes.

Photoanode	R_1 (Ω)	R_2 (Ω)	R_3 (Ω)	R_4 (Ω)
PC31	20.28	1.2	6.4	62.5
PC34	20.59	1.9	19.7	100.6
PC33	20.47	2.3	7.5	10.8
PC35	20.52	1.5	4.8	7.1

4. CONCLUSIONS

TiO_2 nanopowders exhibiting various crystal structures (anatase, rutile and brookite) could to be successfully applied as single layer or bilayer photoanodes in the fabrication of dye-sensitized solar cells. Photoanodes consisting of single layer of anatase TiO_2 crystals result in better solar efficiency as compared to the single layer photoanodes formed from binary and ternary phases. Bilayer photoanodes yield an increase in solar efficiency compared to single layer photoanodes. Increase in efficiency using bilayer photoanodes is attributed to good match of the two films that increases performance of the cell by enhancing charge transfer. The fast charge transfer inside the binary photoanode is also confirmed by EIS analysis. Besides charge transfer, synergistic effect of anatase and rutile mixture, large surface area of porous nanoparticles and efficient light scattering are considered to be effective for enhanced efficiency.

ACKNOWLEDGEMENTS

A grant by the Scientific and Technological Council of Turkey (TUBITAK) through Project number 216M391 is greatly acknowledged.

REFERENCES

[1] Small Spacecraft Technology State of the Art, Mission Design Division, Ames Research Center, Moffett Field, California, 2015, NASA/TP–2015–216648/REV1.

[2] Jean J, Brown PR, Jaffo RL, Buonassisi T, Bulović V. Pathways for solar photovoltaics, Energy and Environ Sci 2015; 4.

[3] O'Regan B, Gratzel M. A low-cost, high efficiency solar cell based on dye-sensitized colloidal TiO_2 films. Nature 1991; 353: p.737.

[4] Ye M, Wen X, Wang M, Locozzia J, Zhang N, Lin C, Lin Z. Recent advances in dye-sensitized solar cells: from photoanodes, sensitizers and electrolytes to counter electrodes. Materials Today 2015; 18: 3.

[5] Li G, Richter CP, Milot RL, Cai L, Schmuttenmaer CA, Crabtree RH, Brudvig GW, Batista VS. Synergistic effect between anatase and rutile TiO_2 nanoparticles in dye-sensitized solar cells. Dalton Trans., 2009; p.10078.

[6] Lekphet W, Ke TC, Su C, Li WR. Morphology control studies of TiO2 microstructures via surfactant-assisted hydrothermal process for dye-sensitized solar cell applications. Applied Surface Science 2016; 382: p. 15.

[7] Shen Z, Wang G, Tian H, Sunarso J, Liu L, Liu J, Liu S. Bi-layer photoanode films of hierarchical carbon-doped brookite-rutile TiO_2 composite and anatase TiO_2 beads for efficient dye-sensitized solar cells. Electrochimica Acta 2016; 216: p. 429.

[8] Liu G, Yan X, Chen Z, Wang X, Wang L, Lu GQ, Cheng HM. Synthesis of rutile–anatase core–shell structured TiO_2 for photocatalysis. J Mater Chem 2009; 19: p.6590.

[9] Erdogan N, Ozturk A, Park J. Hydrothermal synthesis of 3D TiO2 nanostructures using nitric acid: characterization and evolution mechanism. Ceram Int 2016; 42: p. 5985.

[10] Ito S, Chen P, Comte P, Nazeeruddin MK, Liska P, Péchy P, Grätzel M. Fabrication of screen-printing pastes from TiO_2 powders for dye-sensitised solar cells. Prog Photovolt 2007; Res. Appl; 15: 603.

[11] Yu H, Pan J, Bai Y, Zong X, Li X, Wang L. Hydrothermal Synthesis of a Crystalline Rutile TiO2 Nanorod Based Network for Efficient Dye-Sensitized Solar Cells. Chem Eur J 2013; 19: p.13569.

[12] Kambe S, Nakade S, Wada Y, Kitamura T, Yanagida S. Effects of crystal structure, size, shape and surface structural differences on photo-induced electron transport in TiO_2 mesoporous electrodes. J Mater Chem 2002; 12: p.723

[13] Wang Q, Moser, JE, Grätzel M. Electrochemical Impedance Spectroscopic Analysis of Dye-Sensitized Solar Cells. J Phys Chem B 2005; 109: p.14945.